

AIP | Applied Physics Letters

Reversible electron pumping and negative differential resistance in two-step barrier diode under strong terahertz ac field

G. Murillo, P. A. Schulz, and J. C. Arce

Citation: *Appl. Phys. Lett.* **98**, 102108 (2011); doi: 10.1063/1.3562309

View online: <http://dx.doi.org/10.1063/1.3562309>

View Table of Contents: <http://apl.aip.org/resource/1/APPLAB/v98/i10>

Published by the [AIP Publishing LLC](http://www.aip.org).

Additional information on Appl. Phys. Lett.

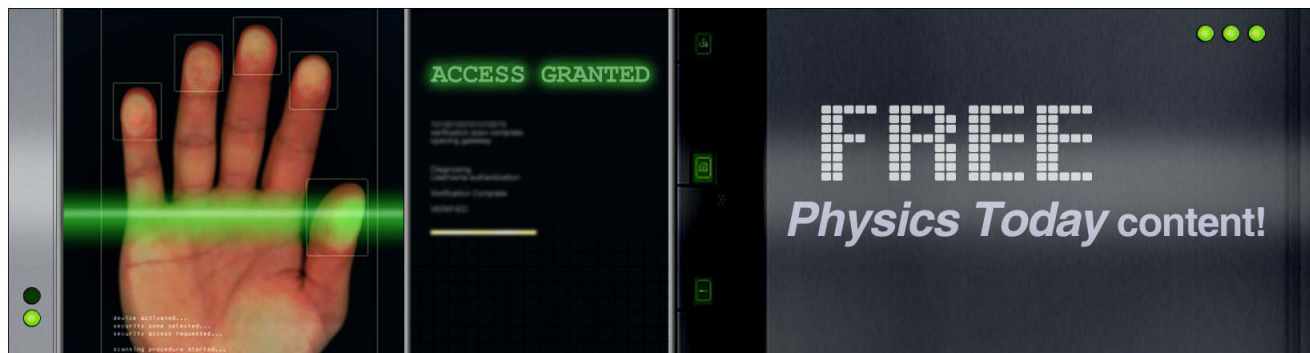
Journal Homepage: <http://apl.aip.org/>

Journal Information: http://apl.aip.org/about/about_the_journal

Top downloads: http://apl.aip.org/features/most_downloaded

Information for Authors: <http://apl.aip.org/authors>

ADVERTISEMENT



Reversible electron pumping and negative differential resistance in two-step barrier diode under strong terahertz ac field

G. Murillo,^{1,a)} P. A. Schulz,^{2,b)} and J. C. Arce^{3,c)}

¹*Departamento de Física, Universidad del Valle, A.A. 25360, Cali, Colombia*

²*Instituto de Física Gleb Wataghin, Universidade Estadual de Campinas, Campinas, Brazil and Faculdade de Ciências Aplicadas, Universidade Estadual de Campinas, 13484-350, Limeira SP, Brazil*

³*Departamento de Química, Universidad del Valle, A.A. 25360, Cali, Colombia*

(Received 2 September 2010; accepted 15 February 2011; published online 9 March 2011)

A computational study, employing a Floquet-transfer-matrix approach, of the current in a model two-step barrier diode under intense ac fields in the terahertz range is reported. It is demonstrated that the field pumps a net tunnel current through the structure, which can exhibit a negative differential resistance and whose direction can be controlled by the ac-bias amplitude. These behaviors are seen to originate from the inelastic scattering of incoming electrons by absorption or emission of field quanta from a shape resonance present in the field-free structure. © 2011 American Institute of Physics. [doi:10.1063/1.3562309]

The negative differential resistance (NDR) (Refs. 1 and 2) and electron pumping^{3,4} phenomena in nanoscopic structures have attracted a great deal of attention, due to their interesting physics and potential technological applications. Double-barrier quantum-well diodes¹ and other low-dimensional systems with spatial reflection symmetry cannot exhibit ac NDR or electron pumping unless such symmetry is broken in some way, for example, by the additional application of a small dc bias.⁵

Schulz and Gonçalves da Silva proposed a two-step barrier diode (TSBD), where the symmetry is intrinsically broken, in principle capable of displaying NDR and electron pumping under an ac field, without the need to apply a voltage.^{6,7} Figure 1(a) illustrates such TSBD built in the layered structure GaAs/Al_xGa_{1-x}As/Al_yGa_{1-y}As/GaAs, with the AlGaAs barriers 100 Å thick (100 Å = 1 a*) and the Al concentrations x and y chosen such that the barrier heights are 150 and 300 meV. Figure 1(b) displays the field-free and two dc transmission coefficients. It is observed that this quantity increases by several orders of magnitude along the sequence reverse-bias → zero-bias → forward-bias. In addition, it is observed that the curves exhibit a resonance feature whose sharpness increases along the same sequence. The first observation is easily understood by noting that the barrier heights decrease along this sequence. The second observation can be explained with the aid of Fig. 2, which shows the probability densities of the continuum states located at the energies of the two strongest features: it can be appreciated that the zero-bias feature is a shape (nontunneling) resonance associated with a state above the first barrier, while the forward-bias feature is a tunneling resonance associated with the metastable triangular Stark well generated in the structure.⁸ The feeble feature at reverse bias must be a remnant of the zero-bias shape resonance.

It is now demonstrated numerically that, indeed, the TSBD can exhibit the ac electron pumping and NDR phenomena, by determining the conductance response of this

structure to ac fields in the terahertz range. The transmission coefficient as a function of incident electron energy and field amplitude and frequency is determined by combining the Floquet approach with the transfer-matrix method.⁹⁻¹⁴ The model uses the following considerations: The impurity concentration is very low, which implies that charge accumulation or depletion layers do not arise at the interfaces; the current density is low enough so that the electrons can be regarded as independent; consistently with the previous considerations, the electron-field scattering is coherent. A large number of incident and outgoing Floquet modes are taken into account, with two adjacent modes separated by an energy $\hbar\omega$, with ω the angular frequency of the ac field.¹³ The

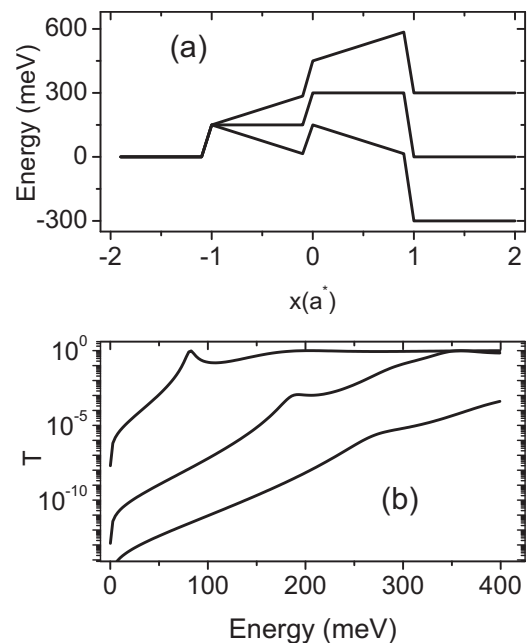


FIG. 1. (a) Band edge of the TSBD under zero bias (center), forward 300 meV bias (bottom), and reverse 300 meV bias (top). (b) The respective transmission coefficients, T . Under zero bias (center curve), a shape (nontunneling) resonance appears at $E_S^R = 190$ meV. Under forward bias (top curve) a tunneling resonance associated with the triangular well arises at $E_T^R = 76$ meV.

^{a)}Electronic mail: gmurillo@uao.edu.co.

^{b)}Electronic mail: pschulz@ifi.unicamp.br.

^{c)}Electronic mail: jularce@univalle.edu.co.

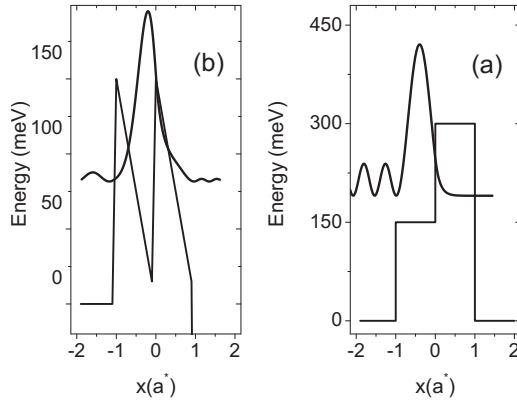


FIG. 2. Probability densities associated with (a) the shape resonance under zero bias and (b) the tunneling resonance under forward 300 meV bias.

layers are denoted as I for $x < 0$ (emitter), II for $0 < x < a$ (first step), III for $a < x < b$ (second step), and IV for $x > b$ (collector). The effective masses, μ , of these layers are

$$\Psi_j = \sum_{m=-\infty}^{\infty} e^{-(iE_m t/\hbar) - (ieF^j x \sin \omega t/\hbar \omega) + [i(eF^j)^2 x \sin 2\omega t/8\hbar \mu^j \omega^2] - (iU \sin \omega t/\hbar \omega)} \times [a_j^m e^{iq_m^j(x - eF^j \cos \omega t/\mu^j \omega^2)} + b_j^m e^{-iq_m^j(x - eF^j \cos \omega t/\mu^j \omega^2)}], \quad (2)$$

where the corresponding wave vector is given by

$$q_m^j = \sqrt{\frac{2\mu^j}{\hbar^2} \left[E - \frac{(eF^j)^2}{4\mu^j \omega^2} + m\hbar \omega - V_{0j} \right]} \quad (3)$$

with V_{0j} the original barrier heights and j labeling the different regions. To ensure convergence, in all cases the summations of Eqs. (1) and (2) are truncated to N values higher than the ratio between the ac bias amplitude and the quantum of energy, $N > eFa^*/\hbar\omega$.

The appropriate boundary conditions lead to an infinite system of algebraic equations relating the coefficients of incident and outgoing waves on each side of an interface p , which can be written as

$$\begin{pmatrix} \tilde{A}_{j+1}^n \\ \tilde{B}_{j+1}^n \end{pmatrix} = \tau_{L \rightarrow R}^p \begin{pmatrix} \tilde{A}_j^n \\ \tilde{B}_j^n \end{pmatrix}, \quad (4)$$

where $\tau_{L \rightarrow R}^p$ is the transfer matrix from left to right. The total transfer matrix across the entire structure is given by

$$\tau_{L \rightarrow R} = \tau_{L \rightarrow R}^0 \tau_{L \rightarrow R}^p \tau_{L \rightarrow R}^{p+1} \cdots \tau_{L \rightarrow R}^N, \quad (5)$$

where $\tau_{L \rightarrow R}^0$ and $\tau_{L \rightarrow R}^N$ are the transfer matrices at the right and left ends of the structure.¹⁵

The conductance in a given direction is $G = (2e^2/h)T$, with T the total transmission coefficient in the same direction, which, in turn, can be obtained by adding the corresponding transmission probabilities of all the channels n ,

$$T = \sum_m \sum_n \frac{k_{\text{out}}^n}{k_L^{\text{in}}} J_{m-n}^2 \left(\frac{eFa^*}{\hbar \omega} \right) \left| \frac{A_R^n}{A_L^0} \right|^2, \quad (6)$$

where J_n is the n th order Bessel function of the first kind.

Figure 3 shows the calculated left \rightarrow right and right

0.067 m_0 , 0.0836 m_0 , 0.1002 m_0 , and 0.067 m_0 , respectively. The ac bias is considered to affect region IV only through a homogeneous modulation, whereas regions II and III both through dipolar and homogeneous modulations, $V(x, t) = [(eFx/2) + (eFa^*/2)] \cos \omega t$ with F the electric field amplitude.^{13,14} Region I is taken as free of modulation to set a convenient energy reference.

The wave function in a constant-potential region has the form^{13–15}

$$\Psi_j = \sum_{n=-\infty}^{\infty} (A_j^n e^{ik_n x} + B_j^n e^{-ik_n x}) e^{-iE_n t/\hbar}, \quad (1)$$

where A_j^n and B_j^n are the probability amplitudes of incoming and outgoing waves, respectively, $k_n = \sqrt{(2\mu E_n)/\hbar^2}$ is the wave number, and $E_n = E \pm n\hbar\omega$ with E the energy of the incident electron and $n = \pm 1, \pm 2, \dots, \pm N$. On the other hand, in regions under homogeneous and dipole-type oscillations, the solutions have the form^{13–15}

\rightarrow left transmission coefficients as functions of incident electron energy for increasing ac bias amplitude and at a fixed frequency (≈ 20 THz). For electrons with energies below the original barrier, the following characteristics are observed: First, the left \rightarrow right and right \rightarrow left transmission coefficients are about equal at low ac bias while at large ac bias the former becomes larger than the latter, as expected from the

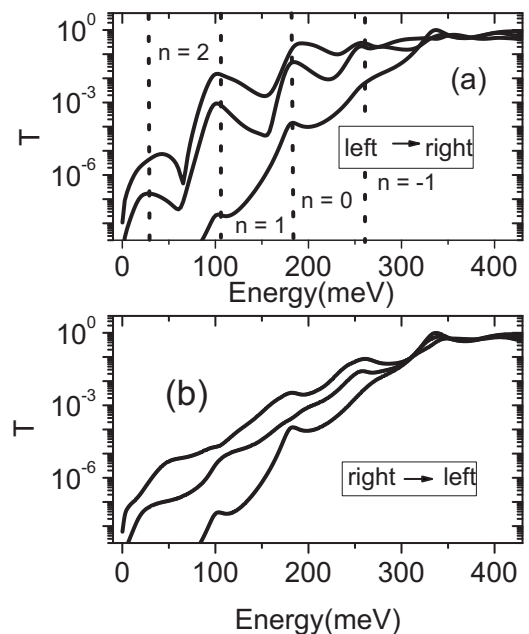


FIG. 3. Left \rightarrow right (a) and right \rightarrow left (b) transmission coefficients as functions of the incident electron energy for $eFa^* = 10, 150$, and 300 meV (from bottom to top) and $\hbar\omega = 80$ meV. The vertical lines indicate the positions of n -quanta replicas of the shape resonance.

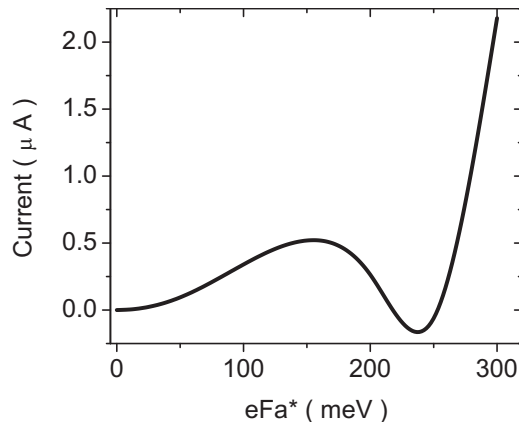


FIG. 4. Net current as a function of the ac bias amplitude.

shape of the potential. Second, both transmission coefficients increase very rapidly with the ac bias amplitude. Third, in the left→right transmission coefficient new strong features show up that are absent in the field-free case; the corresponding features in the right→left transmission coefficient are weak or absent. The peaks can be attributed to the absorption or emission of field quanta from the shape resonance, satisfying the approximate resonance condition $E = E_S^R + n\hbar\omega$, as indicated in Fig. 3. In an experiment, these features will manifest only if the field frequency is greater than the inverse of the lifetime of the resonant state in the heterostructure.¹⁶

The net current, which is the experimentally measurable quantity, is given by

$$I = \frac{2e}{h} \int_0^\infty W(E)(T_{L \rightarrow R} - T_{R \rightarrow L})dE, \quad (7)$$

where $W(E)$ is a time-averaged distribution function, which plays a role analogous to the Fermi distribution appropriate in the dc situation. The determination of such function is a problem in nonlinear response theory which lies beyond the scope of this report. Here, for simplicity, we assume that it is constant in the energy range of interest. Moreover, for convenience, the calculations were performed taking $W(E)=1$. Thus, the following results have only qualitative value. Figure 4 displays the calculated net current as a function of the ac bias amplitude. It is observed that this curve exhibits the NDR phenomenon in the bias range corresponding to energies around the energy of the field-free shape resonance, analogously to what happens in the dc case.¹ In addition, it is seen that the current flows to the right for most of the bias

range, except between 220 and 260 meV where it flows to the left.

The following conclusions can be drawn from the results of this work: First, the application of an intense high-frequency ac field to the TSBD induces a net current, i.e., this device can function as an electron pump. Second, the present results strongly suggest that the direction of such pumping can be controlled by varying the ac bias amplitude. Third, the ac-induced current can exhibit the NDR phenomenon. Four, in the high-frequency ac situation n -quanta replicas of a shape resonance can play a role analogous to the one played by tunneling resonances in the dc situation. The authors hope that the results of these model calculations up to 20 THz will motivate further investigations in high-frequency operation of resonant tunneling diodes.¹⁷

G.M. acknowledges funding from Programa de Doctorados Nacionales 2005 Colciencias and thanks Departamento de Física da Materia Condensada, Universidade Estadual de Campinas, Brazil, for hospitality during an internship in 2008. J.C.A. acknowledges funding from Colciencias under Contract No. 1106-45-221296. P.A.S. acknowledges partial support from CNPq, Brazil.

¹L. L. Chang, L. Esaki, and R. Tsu, *Appl. Phys. Lett.* **24**, 593 (1974).

²For example, M. Rinkö, A. Johansson, V. Kotimäki, and P. Törmä, *ACS Nano* **4**, 3356 (2010).

³D. J. Thouless, *Phys. Rev. B* **27**, 6083 (1983).

⁴M. Switkes, C. M. Marcus, K. Campman, and A. C. Gossard, *Science* **283**, 1905 (1999).

⁵T. C. L. G. Sollner, E. R. Brown, and W. D. Goodhue, *Picosecond Electronics and Optoelectronics Technical Digest* (Optical Society of America, Washington, DC, 1987), Vol. 87, p. 143.

⁶P. A. Schulz and C. E. T. Gonçalves da Silva, *Appl. Phys. Lett.* **52**, 960 (1988).

⁷S. J. Wang, J. C. Lin, W. R. Liou, Y. C. Luo, and C. Y. Cheng, *Appl. Phys. Lett.* **68**, 3320 (1996).

⁸M. L. Zambrano and J. C. Arce, *Phys. Rev. B* **66**, 155340 (2002).

⁹C. Pérez del Valle, R. Lefebvre, and O. Atabek, *Phys. Rev. A* **59**, 3701 (1999).

¹⁰C. Pérez del Valle, R. Lefebvre, and O. Atabek, *J. Phys. B* **34**, 1115 (2001).

¹¹N. Moiseyev and R. Lefebvre, *Phys. Rev. A* **64**, 052711 (2001).

¹²G. Zhou and Y. Li, *J. Phys.: Condens. Matter* **17**, 6663 (2005).

¹³W. Li and L. E. Reichl, *Phys. Rev. B* **62**, 8269 (2000).

¹⁴W. Li, L. E. Reichl, and B. Wu, *Phys. Rev. E* **65**, 056220 (2002).

¹⁵G. Platero and R. Aguado, *Phys. Rep.* **395**, 1 (2004).

¹⁶D. G. Sokolovskii and M. Yu. Sumetski, *Theor. Math. Phys.* **64**, 802 (1985).

¹⁷M. Asada, S. Susuki, and N. Kishimoto, *Jpn. J. Appl. Phys.* **47**, 4375 (2008).